CHEMISTRY OF MATERIALS

ARTICLE

pubs.acs.org/cm

Cobalt−Zinc Molybdates as New Blue Pigments Involving Co^{2+} in Distorted Trigonal Bipyramids and Octahedra

L. Robertson, M. Duttine, M. Gaudon, and A. Demourgues*

Institut de Chimie de la Matière Condensée de Bordeaux-CNRS, Université Bordeaux, 87 Avenue du Dr. A. Schweitzer, 33608 Pessac cedex, France

ABSTRACT: $Zn_{1-x}Co_xMoO_4$ ($x < 0.3$) compounds prepared by the solid-state route crystallize in a triclinic unit cell with the $P\bar{1}$ space group. X-ray diffraction and Rietveld analyses reveal the occurrence of three highly distorted sites with equal occupancies corresponding to one trigonal bipyramidal CoO_5 group and two octahedral CoO_6 groups occupied by either Zn^{2+} or Co^{2+}. Mo^{6+} ions are located in distorted tetrahedral sites. Electron paramagnetic resonance analysis allows characterization of the two kinds of environments with orthorhombic distortion related to two signals with different g values. The UV−vis spectra exhibit intense Co^{2+} d−d transitions associated with CoO_5 and CoO_6 chromophores between 1.9 and 2.6 eV in the visible domain and O−Mo charge transfer at the frontier between the UV and visible ranges. A blue-transmitted window can then be displayed. The formation of covalent MoO_4 entities and polarizable Zn^{2+} cations creating highly distorted noncentrosymmetric sites partially occupied by Co^{2+} allows stabilization of the first blue pigment without Co^{2+} in the tetrahedral environment. Moreover, only 5−10% cobalt is necessary to get a strong blue hue because of the highly distorted sites leading to very important oscillator strengths.

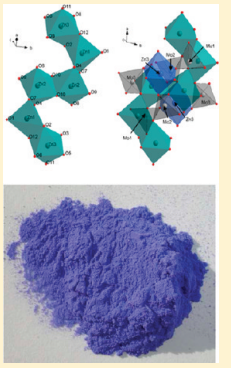

KEYWORDS: cobalt, molybdates, structure, local environments, d−d transitions, blue pigment

INTRODUCTION

Numerous $Co^{2+}(3d^7)$-based oxides exhibit strong violet or blue coloration as well as a light pink hue and have been used as a ceramic pigment.[1] The UV−vis−NIR absorption properties are strongly related to the structural features and more especially to the local environment of transition metals. Zn^{2+} and Co^{2+} are often associated[2] to dilute Co^{2+} cations, which can be considered as a toxic element but also because the chemical properties of both of these elements are close. The crystal field of Co^{2+} can increase from 0.5 eV in a tetrahedral environment to 0.8−1.3 eV in 5-fold or octahedral coordination,[3−5] leading to various d−d transitions on the basis of the Tanabe−Sugano diagrams. Tetrahedral coordination of Co^{2+} is often preferred to octahedral coordination and leads to a strong blue color in $(Co,Zn)Al_2O_4$ spinel[6] or green coloration in ZnO:Co wurtzite for instance.[7] In this last compound, the O−Zn charge transfer band appears at the frontier between the UV and visible ranges whereas the d−d transition of Co^{2+} in tetrahedral coordination occurs around λ = 600 nm (2 eV). Furthermore, if we take the example of silicates, $(Zn,Co)_2SiO_4$ willemite with 30% Co^{2+} (molar concentration) exhibits a strong blue coloration because of the occurrence of Co^{2+} in tetrahedral coordination.[8−10] A light pink or violet hue is associated with Co^{2+} in octahedral coordination. Violet coloration can be found in cobalt phosphates such as $Co_3(PO_4)_2$,[5] where Co^{2+} can occupy either highly distorted 5-fold coordinated or octahedral sites.[11] Dark purple coloration is found in the adamite-type family, such as phosphates $(Zn,Co)_2(OH)PO_4$.[12] As for these phosphates, the arsenates $(Mg,Co)_2(OH)AsO_4$ exhibit vertex- and edge-sharing MO_6, MO_5, and $P(As)O_4$ environments.[4] Transition metals can occupy either highly distorted octahedral or trigonal bipyramidal coordination, but electron paramagnetic resonance (EPR) analysis reveals that Co^{2+} has a strong preference for the octahedral site.[4,13] The occurrence of noncentrosymmetric sites and the presence of O^{2-}/OH^- in the vicinity of Co^{2+} leads to a strong absorption coefficient in the visible range.[4] Finally, violet coloration can also be found in Co_2SiO_4 olivine, where Co^{2+} cations occupy two various distorted octahedral sites.[14]

Then, before this work, the only way to get a blue pigment with Co^{2+} was to stabilize this transition metal in the tetrahedral environment. The comparison of the Co^{2+} crystal field for distorted octahedral sites in $Co_3(PO_4)_2$ and $Co_2(OH)AsO_4$ equal to 1.15 eV[5] and 0.97 eV,[4] respectively, shows that the crystal field and consequently color can be tuned by changing the XO_4 chemical entities and its covalency. After investigation of phosphates, arsenates, or silicates where X−O chemical bonding in XO_4 tetrahedra (X = Si, P, As) is covalent, molybdates have been considered for which two allotropic forms (β, α) corresponding to the $CoMoO_4$ composition can be stabilized.[15,16] Due to the contribution of the O−Mo charge transfer band at the frontier between the UV and visible ranges, which depends on the local environment of Mo^{6+} cations in octahedral (α) or tetrahedral (β) sites, α-$CoMoO_4$ appears green whereas the β-phase is still violet. However, in this case, Mo−O chemical bonds are less covalent than X−O (X = Si, P, As) chemical bonds. Taking into account competitive bonds, the local environment of Co^{2+} will become more covalent in molybdates, leading to a reduction of the crystal field in octahedral symmetry

Received: January 26, 2011
Revised: March 25, 2011
Published: April 13, 2011

and influencing the color of such compounds. Moreover, the site distortion will be affected. As the α/γ-$CuMoO_4$ phase, the β (α) high-temperature/low-pressure form exhibits MoO_4 tetrahedra while the α (γ) low-temperature/high-pressure variety contains MoO_6 octahedra.[17−19] In the case of Co^{2+}, these cations remain in distorted octahedral sites in both β and α forms, where, for $ZnMoO_4$ or α-$CuMoO_4$, M^{2+} cations occupy either distorted trigonal bipyramidal or octahedral coordination.[20,21] As in $(Zn,Co)_2(OH)PO_4$ phosphates or $(Mg,Co)_2(OH)AsO_4$ arsenates, where both these noncentrosymetric sites can be occupied by Co^{2+} cations, we wondered if the solid solutions $(Zn,Co)MoO_4$ can be stabilized with a small amount of Co^{2+} substituted for Zn^{2+}. The polarizable character of Zn^{2+} cations will also affect the site distortion. Finally, the other question was about the UV−vis−NIR optical absorption spectra and if the violet coloration will still be obtained in this series. Powder X-ray diffraction (XRD) analysis and Rietveld refinement have been performed. UV−vis−NIR optical absorption spectra and EPR analyses will be carried out to get information about the Co^{2+} local environments in this solid solution.

EXPERIMENTAL SECTION

Synthesis. $Zn_{1-x}Co_xMoO_4$ powders with the $P\bar{1}$ space group ($x < 0.3$) and $C2/m$ space group associated with β/α allotropic forms ($x \geq 0.5$) were prepared by solid-state reaction from stoichiometric amounts of MoO_3 (Sigma, 99.5%), Co_3O_4 (Alfa Aesar, 99.7%), and ZnO (Aldrich, 99.9%). A mixture of the reactant was heated in an alumina crucible at 700 °C for 20 h and at 800 °C for 10 h and then cooled to room temperature. The $Zn_{1-x}Co_xMoO_4$ powders ($C2/m$ space group, $x \geq 0.5$) corresponding to the α-phase were obtained after the corresponding β-phase powders were milled in an agate mortar. In the $Zn_{1-x}Co_xMoO_4$ solid solutions ($x \geq 0.5$), the β-phase was a minor compound.

Powder X-ray Diffraction and Refinement Procedure. Powder X-ray diffraction patterns were recorded on a Philips PW 1820 apparatus equipped with a $K\alpha_1/K\alpha_2$ source and a copper anticathode. Diffraction patterns were collected with a 2θ step of 0.02° with a counting time of 10 s per step in routine mode. For Rietveld analysis,[22] monochromatic Cu $K\alpha_1$ radiation was used with a 2θ step of 0.015° and a counting time of over 200 s per step with $8° \leq 2\theta \leq 120°$. Diffractograms were refined via a whole pattern matching procedure using the FULLPROF program package. Background parameters, zero, peak profiles, and unit cells were refined in the first step. All the atomic positions and the partial Zn^{2+}/Co^{2+} occupancies on each of the three atomic positions were refined in the second step. Isotropic thermal displacements were fixed at the beginning of the refinement, and all the atomic positions were fully occupied with a partial occupancy of Zn^{2+} and Co^{2+} on the same crystallographic sites. The isotropic thermal displacement was also refined in the third step by considering three different values for A^{2+}, Mo^{6+}, and O^{2-} crystallographic sites. In the final step, the Zn^{2+}/Co^{2+}, Mo^{6+}, and O^{2-} isotropic thermal displacements as well as the three Zn^{2+}/Co^{2+} partial occupancies in each site and all the atomic positions were simultaneously refined. Refined profiles and structural parameters are reported.

Diffuse Reflectance Spectroscopy. Diffuse reflectance spectra $R(\lambda)$ were recorded at room temperature from 210 to 2500 nm with a step of 1 nm on a Cary 17 spectrophotometer using an integration sphere. Halon was used as the white reference for the blank. All diffuse reflectance spectra $R(\lambda)$ are represented after Kubelka−Munk treatment, $(1 - R^2)/2R$ versus energy (eV), and correspond to optical absorption spectra. In this approximation, we considered that particle sizes are about 5 times the analyzed wavelength domain (400−2500 nm). To identify optical absorption transitions, we considered also in a first approximation that the absorption spectrum in the vis−NIR region is the sum of several Gaussian functions corresponding to each d−d transition. Only the UV−vis−NIR wavelength range and the La^*b^* space parameters (L = luminosity, a^* = green to red axis, and b^* = yellow to blue axis coefficients) are discussed in this paper. No mathematical treatment has to be conducted since the apparatus directly gives La^*b^* chromatic parameters.

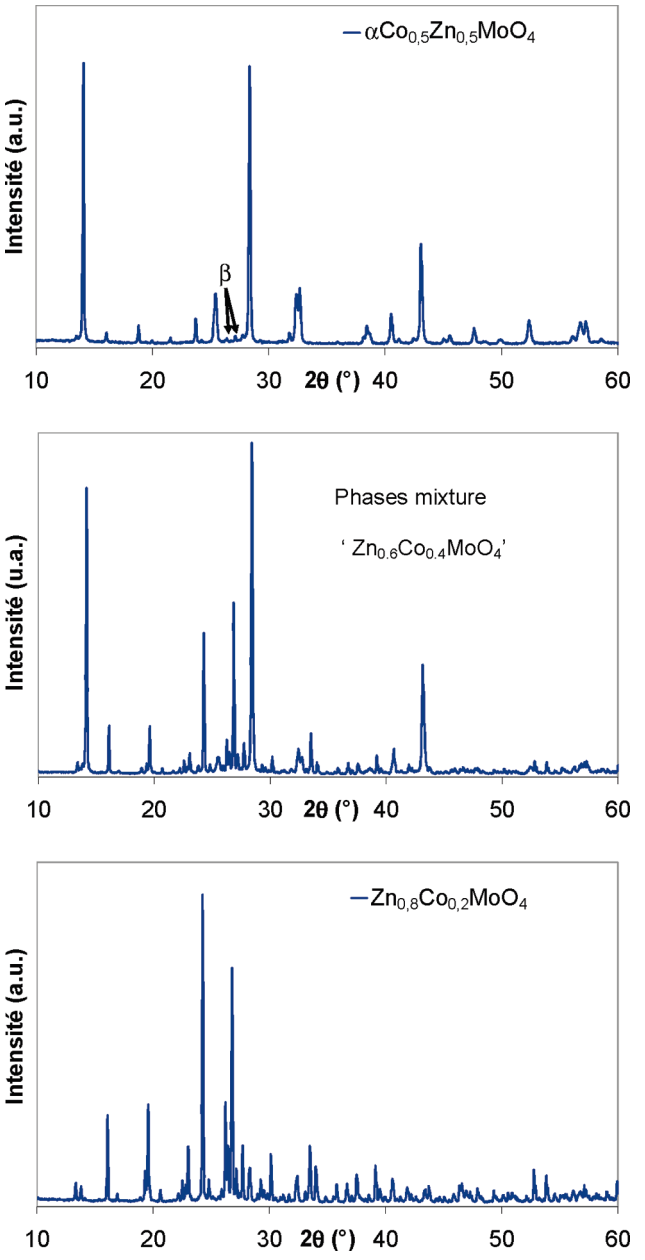

Figure 1. XRD patterns of α-$Zn_{0.5}Co_{0.5}MoO_4$ ($C2/m$), a phase mixture corresponding to the $Zn_{0.6}Co_{0.4}MoO_4$ composition, and $Zn_{0.8}Co_{0.2}MoO_4$ ($P\bar{1}$).

EPR Measurements. Electron paramagnetic resonance spectra were recorded from room temperature to $T = 5$ K with a Bruker EMX spectrometer at X-band frequency (9.45 GHz) to identify the Co^{2+} local environments. The SIMFONIA program was used to simulate th eEPR spectra and give rise to the determination of g values and hyperfine interaction parameters.

dx.doi.org/10.1021/cm200795p |Chem. Mater. 2011, 23, 2419–2427

Table 1. Unit Cell Parameters of $Zn_{1-x}Co_xMoO_4$ Compounds ($P\bar{1}$ Space Group, $x < 0.3$)

x(Co)	a (Å)	b (Å)	c (Å)	α (deg)	β (deg)	γ (deg)	V (Å^3)
0.2	8.363(1)	9.680(1)	6.964(1)	106.82(1)	101.73(1)	96.62(1)	519.14(8)
0.1	8.367(1)	9.688(1)	6.965(1)	106.84(1)	101.72(1)	96.68(1)	519.78(8)
0	8.369(1)	9.693(1)	6.965(1)	106.86(1)	101.745(1)	96.75(1)	519.93(8)

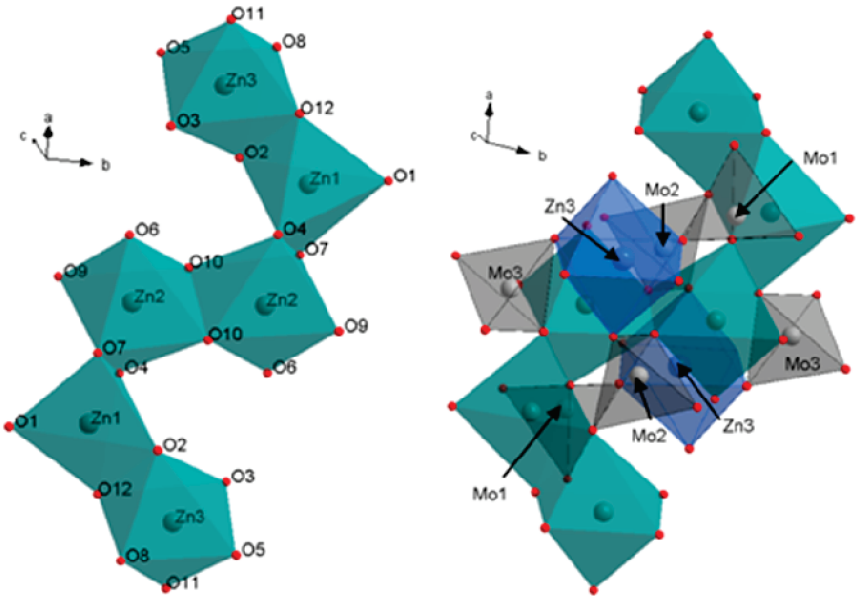

Figure 2. Representation of zigzag chains with $Zn(Co)O_5$ and $Zn(Co)O_6$ edge-sharing polyhedra and perspective view of the $Zn_{1-x}Co_xMoO_4$ (space group $P\bar{1}$) compound.

RESULTS AND DISCUSSION

Structural Features. Cobalt−zinc molybdates with the $Zn_{1-x}Co_xMoO_4$ formula can adopt three various frameworks depending on the x value. The $Zn_{1-x}Co_xMoO_4$ XRD patterns corresponding to three various cobalt rates (x = 0.5, 0.4, and 0.2) are represented in Figure 1. For $x > 0.5$, these compounds crystallize in two monoclinic cells (space group $C2/m$) corresponding to β (high-temperature/low-pressure)/α(low-temperature/high-pressure) allotropic forms associated with the first-order phase transition. $FeMoO_4$, $CoMoO_4$, and $NiMoO_4$ phases adopt the same structural features.[15,16] In these structures, Co^{2+} occupies two distorted octahedral sites. As the Co^{2+} content decreases for $x < 0.5$, another structure appears related to the $ZnMoO_4$-type structure which crystallizes in a triclinic unit cell (space group $P\bar{1}$). The proportion of each phase can be determined by Rietveld analysis taking into account model compounds for x = 0.4 and x = 0.3 and corresponds to 52%/48% (α ($C2/m$)/$P\bar{1}$) and 3%/97%, respectively. The Rietveld fit of the phase mixture corresponding to a Co^{2+} rate equal to x = 0.4 is represented in Figure 3. Then the upper and lower limits of the two solid solutions associated with α $C2/m$ and $P\bar{1}$ space groups can be determined. For $0.5 < x < 1$, the α $C2/m$ phase was stabilized, whereas the pure $P\bar{1}$ phase was obtained for $0 < x < 0.29$. Otherwise ($0.29 < x < 0.5$) the synthesis led to a mixture of these two phases. In this paper, we focus on the synthesis and characterization of the Zn-rich phase with the $P\bar{1}$ unit cell and the correlation between structural features and UV−vis−NIR optical absorption properties. The refined cell parameters reported in Table 1 for x = 0, 0.1, and 0.2 show a slight and gradual decrease of the unit cell volume as the cobalt rate increases. Only the a and b parameters slightly decrease, whereas the c parameter remains constant as the cobalt content increases. In this network represented in Figure 2, Zn^{2+}/Co^{2+} cations are associated in three various crystallographic sites, forming zigzag chains with edge-sharing trigonal bipyramidal and octahedral sites. Mo^{6+} ions are located in tetrahedral sites sharing vertices with Zn^{2+}/Co^{2+} polyhedra. Then the structural parameters of the $Zn_{0.8}Co_{0.2}MoO_4$ compound (cell parameters, atomic positions, isotropic thermal displacements, occupancies) are refined. Observed, calculated, and difference XRD plots are represented in Figure 3. Rietveld data and experimental conditions for data collection are reported in Table 2, and the refined structural parameters are given in Table 3. The three refined isotropic thermal displacements for each ion have an expected value. The three atomic positions associated with A^{2+} (Zn^{2+}/Co^{2+}) cations are fully occupied, and the Co^{2+} rate is refined separately without constraints on each various sites. Surpringly, the total refined Co rate is equal to 0.22(3) and is close to the theoretical value, 0.2, despite the fact that the atomic form factors of Zn^{2+} and Co^{2+} are close and such ions are difficult to differentiate. One should note that the 5-fold-coordinated site (Zn1) corresponding to a trigonal bipyramidal coordination is less occupied by Co^{2+} than the distorted octahedral sites (Zn2 and Zn3) but the Co rate in the Zn1 site remains high. Interatomic distances are given in Table 4. The MoO4 tetrahedra are distorted, and the Mo−O bond distances vary from 1.66(1) to 1.84(1) Å. The

dx.doi.org/10.1021/cm200795p |Chem. Mater. 2011, 23, 2419–2427

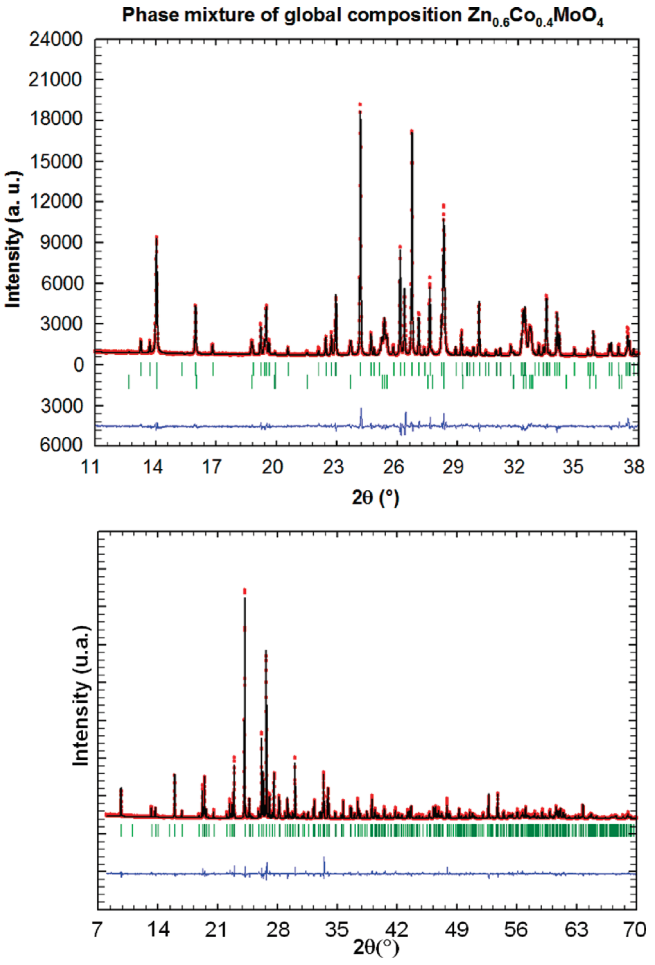

Figure 3. Observed, calculated, and difference X-ray diffraction patterns of the phase mixture (global composition $Zn_{0.6}Co_{0.4}MoO_4$, top) and $Zn_{0.8}Co_{0.2}MoO_4$ (space group $P\bar{1}$, bottom). The tick marks represent the position of the diffraction lines.

Zn1/Co1 trigonal bipyramidal site is highly distorted and smaller than the two distorted octahedral environments. The Zn/Co−O average bond distances in both of these sites vary between 1.97(1) and 2.25(1) Å. All these environments represented in Figure 4 are more distorted in $Zn_{0.8}Co_{0.2}MoO_4$ than in $ZnMoO_4$[20,21] because of the presence of Co^{2+} substituted for Zn^{2+}. Finally, to support the assignment of Co^{2+}/Zn^{2+} in each site, bond valence sum analysis can be considered. Unfortunately, the r_0 constant values $(V_i = \Sigma^i[\exp[(r^o - r_{ij})/B]])^{23}$ of Co^{2+} and Zn^{2+} are close and equal to 1.692 and 1.704 Å, respectively. Then it is impossible to make a conclusion about the site preference of Co^{2+} and Zn^{2+} ions.

UV−Vis−NIR Optical Absorption Properties. Optical absorption spectra of $Zn_{0.8}Co_{0.2}MoO_4$ and β-$CoMoO_4$ are represented in Figure 5 corresponding to the NIR and visible ranges. Deconvolutions into Gaussian functions to identify d−d transitions are given in Figure 6. Electronic transitions and related energy (eV), assigned to octahedral and trigonal bipyramidal sites, are reported in Table 5. The comparison between $Zn_{0.8}Co_{0.2}MoO_4$ and β-$CoMoO_4$ where Mo^{6+} ions occupy tetrahedral sites and Co^{2+} ions are in the distorted octahedral environment, reveal for the $Zn_{0.8}Co_{0.2}MoO_4$ compound two additionnal contributions in the visible region at 1.90 eV and in the near-infrared range at 1.36 eV. For the CoO_6 chromophore, three spin-allowed transitions, $^4T_{1g} \rightarrow {}^4T_{2g}(F)$, $^4T_{1g} \rightarrow {}^4A_{2g}(F)$, and $^4T_{1g} \rightarrow {}^4T_{1g}(P)$, appear at 0.83, 1.68, and 2.12 eV, respectively. On the basis of the Tanabe−Sugano diagram for a d^7 ion in octahedral symmetry, the crystal field has been determined and remains small and equal to 0.85 eV in good agreement with the large Co−O bond distances and CoO_6 site

Table 2. Rietveld Data and Experimental Conditions for Data Collection

formula	$Zn_{0.8}Co_{0.2}MoO_4$
symmetry	triclinic
space group	$P\bar{1}$
unit cell params	a = 8.3625(6) Å, b = 9.6798(6) Å, c = 6.9638(4) Å
	α = 106.823(4)°, β = 101.727(5)°, γ = 96.621(3)°
volume	519.14(8) Å^3
Z	2
D_c	4.30 g·cm^{-3}
radiation	Cu Kα$_1$ (1.54052 Å)
	graphite monochromator
peak shape function	η = 0.65
PV = $\eta L + (1 - \eta)G$	
fwhm function	$H^2 = U \tan^2\theta + V \tan\theta + W$
measuring range	$8° \le 2\theta \le 120°$
no. of reflns collected	1544
no. of params used in refinement	81
cR_p	0.16
cR_{wp}	0.17

Table 3. Atomic Coordinates, Occupancies, and Isotropic Thermal Displacements (Å^2) of $Zn_{0.8}Co_{0.2}MoO_4$

	x/a	y/b	z/c	B_{iso}	occupancy
Mo1	0.0224(3)	0.2981(2)	0.6245(2)	0.30(3)	1.000
Mo2	0.3018(3)	0.3953(2)	0.1585(2)	0.30(3)	1.000
Mo3	0.4962(3)	0.0125(2)	0.2443(2)	0.30(3)	1.000
Zn1	0.0330(5)	0.1137(4)	0.2886(3)	0.65(7)	0.87(3)
Zn2	0.4653(2)	0.3061(4)	0.5110(3)	0.65(7)	0.82(3)
Zn3	0.7508(6)	0.3062(4)	0.0913(3)	0.65(7)	0.65(3)
Co1	0.0330(5)	0.1137(4)	0.2886(3)	0.65(7)	0.13(3)
Co2	0.4653(5)	0.3061(4)	0.5110(3)	0.65(7)	0.18(3)
Co3	0.7508(6)	0.3062(4)	0.0913(3)	0.65(7)	0.35(3)
O1	0.003(2)	0.116(2)	0.715(1)	1.09(9)	1.000
O2	0.059(2)	0.279(2)	0.147(1)	1.09(9)	1.000
O3	0.146(2)	0.485(2)	0.755(1)	1.09(9)	1.000
O4	0.150(2)	0.278(2)	0.490(1)	1.09(9)	1.000
O5	0.268(2)	0.568(2)	0.097(1)	1.09(9)	1.000
O6	0.236(2)	0.704(2)	0.453(1)	1.09(9)	1.000
O7	0.344(2)	0.116(2)	0.302(1)	1.09(9)	1.000
O8	0.338(2)	0.907(2)	0.079(1)	1.09(9)	1.000
O9	0.454(2)	0.130(2)	0.646(1)	1.09(9)	1.000
O10	0.457(2)	0.481(2)	0.352(1)	1.09(9)	1.000
O11	0.452(2)	0.297(2)	0.086(1)	1.09(9)	1.000
O12	0.745(2)	0.124(2)	0.243(1)	1.09(9)	1.000

dx.doi.org/10.1021/cm200795p |*Chem. Mater.* 2011, 23, 2419–2427

Table 4. Interatomic Bond Distances (Å) of $Zn_{0.8}Co_{0.2}MoO_4$

Mo1	O6	1.73(1)	Mo2	O5	1.66 (1)	Mo3	O7	1.67(2)
	O3	1.77(1)		O11	1.70(2)		O8	1.68(1)
	O4	1.79(2)		O2	1.74(1)		O9	1.70 (1)
	O1	1.84(1)		O10	1.84(1)		O12	1.80(1)
Zn1/Co1	O1	1.88(1)	Zn2/Co2	O10	1.97(1)	Zn3/Co3	O3	2.01(1)
	O12	1.95(2)		O6	2.03(2)		O11	2.05(2)
	O2	2.07(2)		O9	2.09(1)		O2	2.12(2)
	O4	2.09 (1)		O4	2.10(2)		O8	2.14(1)
	O7	2.13(1)		O10	2.24(1)		O5	2.19(1)
				O7	2.25 (1)		O12	2.23(2)

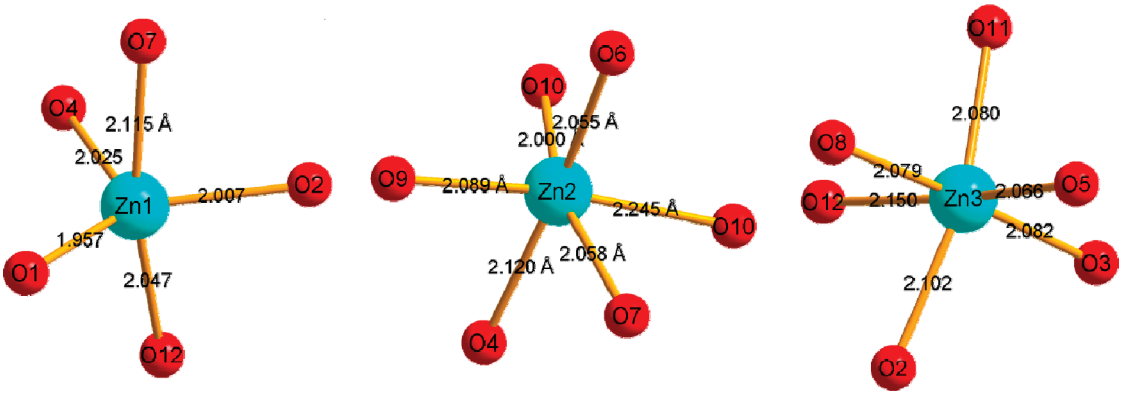

Figure 4. Representation of the three distinct $Zn(Co)O_5$ and $Zn(Co)O_6$ distorted polyhedra in the $Zn_{0.8}Co_{0.2}MoO_4$ compound.

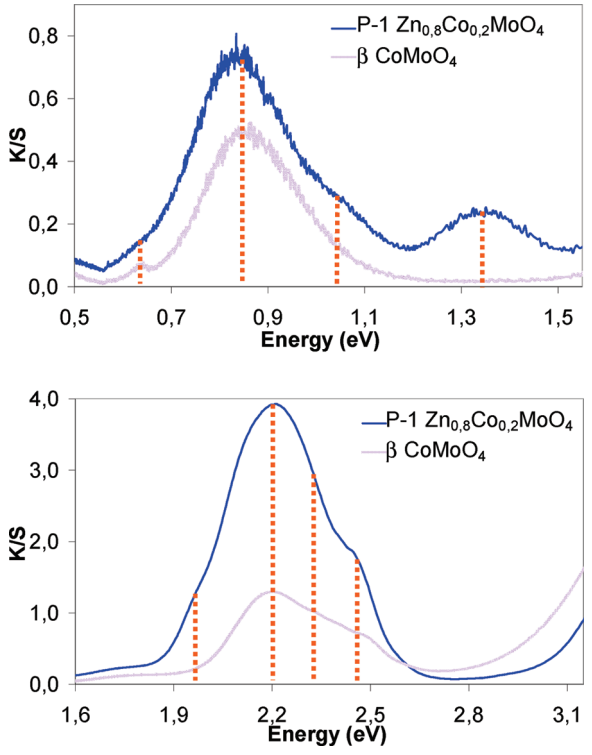

Figure 5. Vis−NIR absorption properties of β-$CoMoO_4$ and $Zn_{0.8}Co_{0.2}MoO_4$ compounds with various electronic transitions.

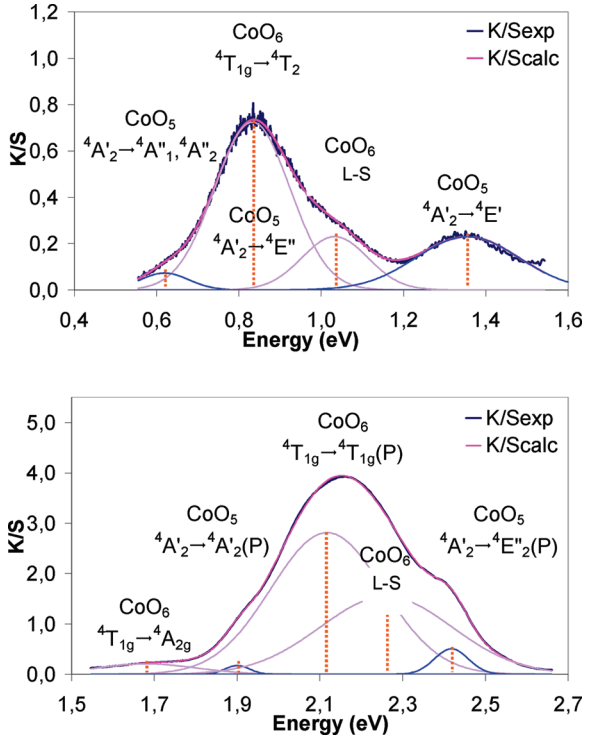

Figure 6. Deconvolution of vis−NIR absorption spectra of the $Zn_{0.8}Co_{0.2}MoO_4$ compound into Gaussian functions related to various electronic transitions for CoO_5 and CoO_6 sites.

size. Additional transitions in the near-infrared and visible regions are associated with $^4T_{1g} \rightarrow {}^4T_{2g}(F)$ and $^4T_{1g} \rightarrow {}^4T_{1g}(P)$ central transitions, respectively. These additionnal transitions are attributed to L−S spin−orbit coupling. In the case of the

dx.doi.org/10.1021/cm200795p |*Chem. Mater.* 2011, 23, 2419–2427

Table 5. Electronic Transitions and Energy Values Associated with CoO_5 and CoO_6 Sites[a]

polyhedron	transition	energy (eV)	param	energy (eV)
O_h CoO[6]	$^4T_{1g} \rightarrow {}^4T_{2g}(F)$	0.83	Δ_0	0.85
	$^4T_{1g} \rightarrow {}^4A_{2g}(F)$	1.68	B	0.087
	$^4T_{1g} \rightarrow {}^4T_{1g}(P)$	2.12	Δ_0/B	9.8

polyhedron	transition	$Co_2(AsO_4)OH$ (ref 4)	$(Mg,Co)_2(AsO_4)OH$ (ref 4)	$Zn_{0.8}Co_{0.2}MoO_4$(this work)
D_{3h} CoO_5	$^4A'_2 \rightarrow {}^4A''_1, {}^4A''_2$	0.62 eV	0.62 eV	0.62 eV
	$^4A'_2 \rightarrow {}^4E''$	0.78 eV	0.80 eV	0.83 eV
	$^4A'_2 \rightarrow {}^4E'$	1.35 eV	1.35 eV	1.36 eV
	$^4A'_2 \rightarrow {}^4A'_2(P)$	1.99 eV	2.00 eV	1.90 eV
	$^4A'_2 \rightarrow {}^4E''_2(P)$	2.46 eV	2.48 eV	2.42 eV

[a] UV−vis−NIR optical absorption spectra represented in Figures 7 and 8.

Table 6. Effective *g* and *A* (Hyperfine Structure Constant) Values Determined by Simulation (SIMFONIA) of EPR Experimental Spectra Recorded at *T* = 5 K (Figures 8 and 9)

compd	ref	site	g_1	g_2	g_3	$\langle g \rangle$	$\lvert A_1 \rvert \times 10^{-4}$ cm^{-1}	$\lvert A_2 \rvert \times 10^{-4}$ cm^{-1}	$\lvert A_3 \rvert \times 10^{-4}$ cm^{-1}
$Zn_{0.995}Co_{0.005}MoO_4$	this work	1	5.79	3.90	3.50	4.40	244	97	82
$Zn_{0.995}Co_{0.005}MoO_4$	this work	2	5.49	3.97	3.59	4.35	203	84	77
$(NH_4)Mg_{0.995}Co_{0.005}(PO_4)\cdot H_2O$	26	O_h	5.7	5.3	2.8	4.6	189	148	<20
$(Mg_{1.99}Co_{0.01})(OH)(AsO_4)$	13	Oh	6.22	4.21	2.87	4.43	240	140	<20
Co:[ZnZn](EDTA)·$6H_2O$	27	O_h	5.80	3.76	3.33	4.30			

Figure 7. Picture of the $Zn_{0.8}Co_{0.2}MoO_4$ compound with associated *Lab* parameters.

$Zn_{0.8}Co_{0.2}MoO_4$ compound, one should note the greater intensity of d−d electronic transitions assigned to Co^{2+} in the highly distorted (noncentrosymmetric) octahedral site due to the enhancement of the oscillator strength. In trigonal bipyramidal Co^{2+} environments, numerous spin-allowed transitions appear, and their assignments and energy values are the following: $^4A'_2 \rightarrow {}^4A''_1, {}^4A''_2$ at 0.62 eV, $^4A'_2 \rightarrow {}^4E''_2$ at 0.83 eV, $^4A'_2 \rightarrow {}^4E'$ at 1.36 eV, $^4A'_2 \rightarrow {}^4A'_2(P)$ at 1.90 eV, and $^4A'_2 \rightarrow {}^4E''_2(P)$ at 2.42 eV. Then, by comparison with the data of $Co_2(AsO_4)OH$ and $(Mg,Co)_2(AsO_4)OH$[4] compounds and transition assignments, the other optical absorption bands have been attributed to CoO_5 chromophores. However, these

dx.doi.org/10.1021/cm200795p |*Chem. Mater.* 2011, 23, 2419–2427

additional bands attributed to CoO_5 sites have lower intensities than those assigned to CoO_6 chromophores. This is probably due to the smaller rate of Co^{2+} in the CoO_5 environment in good agreement with the structure refinement and Co^{2+} occupancies considering in a first approximation that the oscillator strengths of both these sites are comparable. Moreover, these bands attributed to CoO_5 chromophores are more intense in $Co_3(PO_4)_2$ because of the larger rate of Co^{2+} in the 5-fold-coordinated site. Furthermore, the O−Mo charge transfer band (CTB) in $Zn_{0.8}Co_{0.2}MoO_4$ appears at higher energy than the CTB in β-$CoMoO_4$ because the Mo−O chemical bond in zinc molybdate is more covalent. The presence of Zn^{2+} substituted for Co^{2+} contributes indeed by competitive bonds to enhance the covalent character of the Mo−O bond, as explained in the Introduction. Furthermore, the crystal field of highly distorted CoO_6 sites is around 0.85 eV. This value is smaller than those of $Co_3(PO_4)_2$ and $Co_2(OH)AsO_4$, which are equal to 1.15 eV[5] and 0.97 eV,[4] respectively . This result was expected, leading to a gradual shift of d−d transition bands at lower energies. Moreover, the occurrence of Zn^{2+} and Co^{2+} stabilized on the same crystallographic sites, creating disorder and a large range of $A^{2+}-O^{2-}$ bond distances, leads to highly distorted sites with a lower crystal field. Finally, the strong intensities of the absorption bands covering energies between 1.9 and 2.6 eV due to the two CoO_6 and CoO_5 distorted sites and the displacement of the O−Mo CTB to higher energy lead to a beautiful blue pigment with $L = 52.2$, $a = 12.7$, and $b = -45.7$ (Figure 7). Moreover, a cobalt rate between 5% and 10% is sufficient to get a strong blue hue.

EPR Analysis. Considering the high sensitivity of the EPR probe to the local environment, analyses were carried out to have a signature of Co^{2+} in various sites. The aim of this section is just to give a first analysis of the EPR results and to support the structural features of zinc−cobalt molybdates as well as the UV−vis−NIR spectral analysis. X-band EPR measurements were performed at several temperatures between room temperature and $T = 5$ K on two different $Zn_{1-x}Co_xMoO_4$ compositions with low Co^{2+} content ($x = 0.02$ and 0.005) to get high-quality signals by minimizing line broadening due to dipole−dipole coupling. EPR spectra are represented in Figures 8 and 9. Resonance signals appear only at $T < 50$ K because the spin−lattice relaxation time is too short at higher temperatures for octahedral coordination of high-spin-state Co^{2+} and hyperfine structures can be identified at $T < 25$ K. The spectrum at $T = 5$ K, which corresponds to the most intense and well-resolved signals, can be described in terms of an effective spin $S = 1/2$ interacting with the nuclear spin of a single ^{59}Co nucleus ($I = 7/2$). This effective spin is associated with the ground-state Kramer doublet arising in the purely octahedral crystal field from the splitting in the zero field of the orbital triplet state $^4T^1$ ($3d^7$ high-spin) through spin−orbit coupling.[24] In such a case, both **g** and **A** (hyperfine coupling tensor) are isotropic, and the associated g and A values are about 4.3 and about 0.01 cm^{-1}, respectively.[24,25] For Co^{2+} in distorted octahedral sites, **g** and **A** become very anisotropic, and the mean g factor is $\langle g \rangle = 4.3-4.4$ (Table 6) in many cases.[13,26,27] In a previous study on $(Mg,Co)(OH)AsO_4$ arsenate,[6] where Co^{2+} can occupy octahedra or trigonal bipyramids, the EPR signal reveals that Co^{2+} ions occupy only the distorted octahedral site with a large anisotropy of g values ($g_1 = 2.87$, $g_2 = 4.21$, $g_3 = 6.22$) due to high distortion and the presence of both oxygen and hydroxyls in the vicinity of Co^{2+}. This study[6] outlined the strong preference of Co^{2+} for octahedral symmetry.

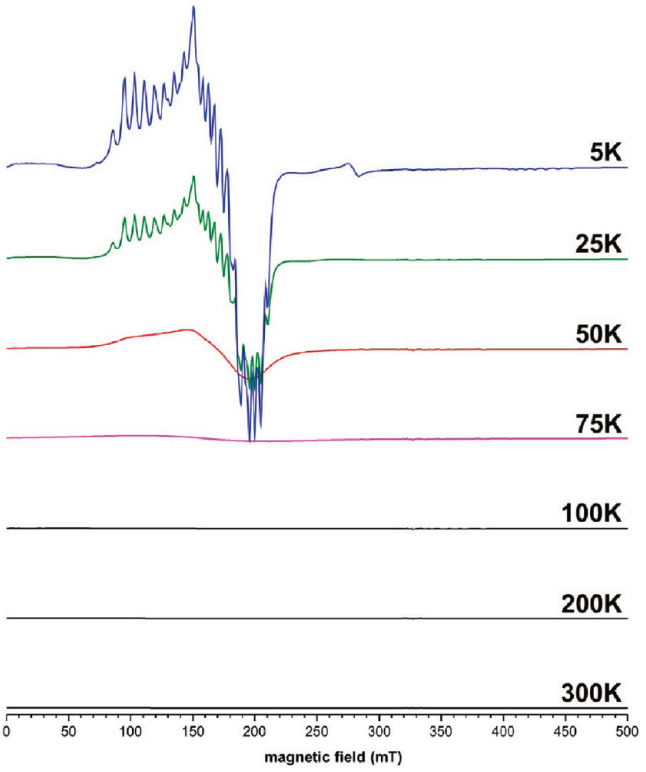

Figure 8. Experimental X-band EPR spectra recorded at various temperatures for the $Zn_{0.98}Co_{0.02}MoO_4$ composition (microwave frequency $n = 9.45$ GHz, microwave power $P = 10$ mW, amplitude of magnetic field modulation MA = 0.6 mT, modulation frequency MF = 100 kHz, spectral resolution SR = 0.5 mT/pt).

Actually, EPR spectra of $Zn_{1-x}Co_xMoO_4$ at $T = 5$ K represented on Figures 8 and 9 reveal the occurrence of two different signals with three components which may correspond to two different sites with strong orthorhombic distortion of octahedral symmetry. For each component, $2I + 1 = 8$ lines are observed because of hyperfine interaction with the ^{59}Co nuclear spin ($I = 7/2$). The simulation of these two signals, using an effective $S = 1/2$ spin model, has given rise to the determination of the effective g and A values reported in Table 6. The g values are $g_1^1 = 5.79 \pm 0.02$, $g_2^1 = 3.90 \pm 0.03$, $g_3^1 = 3.50 \pm 0.02$, $g_1^2 = 5.49 \pm 0.02$, $g_2^2 = 3.97 \pm 0.04$, and $g_3^2 = 3.59 \pm 0.02$, and the effective hyperfine splitting constants are $|A_1^1| = 0.0244 \pm 0.0010$ cm^{-1}, $|A_2^1| = 0.0097 \pm 0.0007$ cm^{-1}, $|A_3^1| = 0.0082 \pm 0.0005$ cm^{-1}, $|A_1^2| = 0.0203 \pm 0.0011$ cm^{-1}, $|A_2^2| = 0.0084 \pm 0.0008$ cm^{-1}, and $|A_3^2| = 0.0077 \pm 0.0006$ cm^{-1}. The mean g factors $\langle g^1 \rangle = 4.40$ and $\langle g^2 \rangle = 4.35$ and the magnitude of A are in good agreement with those observed in other octahedrally coordinated cobalt compounds (Table 6).[13,25,26] The effective g and A values, determined by simulation, are significantly different for both of these signals, and the large anisotropies could originate from the strong distortions observed for CoO_5 and CoO_6 polyhedra where the average Co−O bond distances range from 1.88 to 2.13 Å (CoO_5) and from 1.97 to 2.25 Å (CoO_6). Furthermore, one should point out the rather good agreement between the experimental and theoretical spectra obtained by adding the two simulated signals (Figure 9). The proportion of the two signals, 1/3:2/3, is in good agreement with the occurrence of three kinds of environments for Zn^{2+}/Co^{2+} cations with equal

dx.doi.org/10.1021/cm200795p |*Chem. Mater.* 2011, 23, 2419–2427

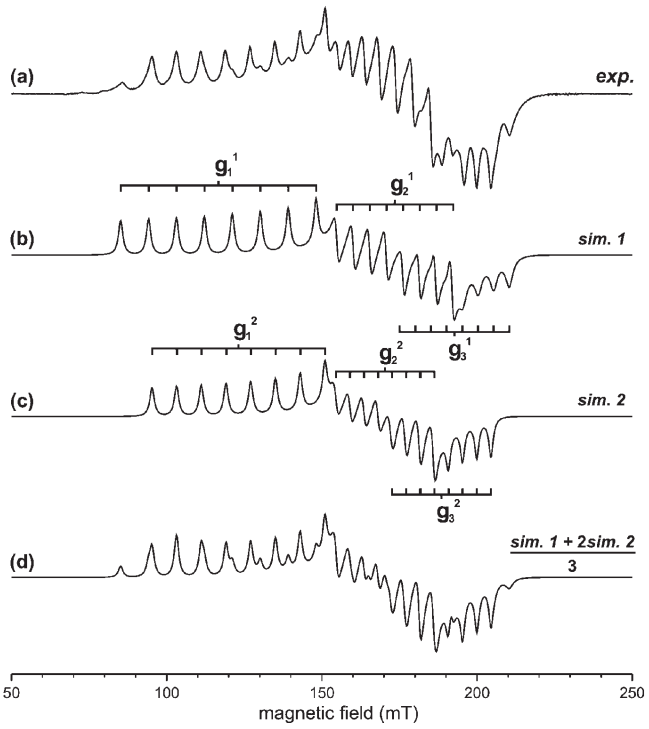

Figure 9. Experimental X-band EPR spectra of $Zn_{0.995}Co_{0.005}MoO_4$ recorded at 5 K (a) and simulated EPR signal of Co^{2+} in (b) site 1 and (c) site 2. (d) Sum of the simulated signals b and c with intensity ratio 1/3:2/3.

occupancies as mentionned in the case of powder XRD analysis. Moreover, UV−vis−NIR investigations also reveal the occurrence of CoO_6 and CoO_5 polyhedra. Thus, EPR signal 1 showing the largest anisotropy of *g* and *A* values, could be associated with the CoO_5 environment and signal 2 with the two distorted octahedra which cannot be differentiated by EPR analysis.

CONCLUSIONS

This is the first example of intense Co^{2+} blue pigment where Co^{2+} ions do not occupy tetrahedral sites but are located in two highly distorted environments related to octahedral and trigonal bipyramidal symmetries. The occurrence of Mo^{6+} creating less covalent MoO_4 tetrahedral sites than the $SiO_4/PO_4/AsO_4$ sites allows enhancement by competitive bonds of the Co−O covalent character and reduction of the Co^{2+} crystal field in the cobalt molybdate series. Moreover, the presence of polarizable Zn^{2+} cations substituted partially for Co^{2+}, creating disorder with a large range of A^{2+}−O^{2-} bond distances, contributes to the generation of more covalent Mo−O bonds than in $CoMoO_4$ and then to a shift to the UV range of the O−Mo charge transfer band. On the basis of XRD data refinement and EPR analyis, the trigonal bipyramidal CoO_5 group as well as the two octhaedral CoO_6 groups appear highly distorted. The bond distances in both of these sites can indeed vary between 1.97(1) and 2.25(1) Å. Three distinct *g* values characteristic of orthorhombic distortions are obtained, and Co^{2+} in trigonal bipyramids are distinguished from Co^{2+} in distorted octahedral sites. Co^{2+} ions are stabilized in these three environments with equal occupancies. For larger cobalt content ($Zn_{0.8}Co_{0.2}MoO_4$), XRD and UV−vis−NIR analyses seem to show the preference of Co^{2+} for octahedral sites but the CoO_5 entity concentration remains high in these molybdates. For a lower Co^{2+} rate, EPR analysis reveals that the Co^{2+} cation contents in these three sites are rougly equivalent. Moreover, because of the site distortion, the oscillator strength remains high and consequently the absorption intensities of d−d transitions are very important. Furthermore, the contribution of CoO_5 sites appears in the red region (1.9 eV) of the visible domain. The O−Mo charge transfer band at the frontier between the UV and visible ranges and in addition the high intensities of the d−d transitions attributed to CoO_5 and CoO_6 chromophores between 1.9 and 2.6 eV are at the origin of this strong blue coloration. Then the occurrence of the MoO_4 tetrahedral site, the influence of the Zn^{2+} site distortion, and the stabilization of Co^{2+} in highly distorted trigonal bipyramidal CoO_5 and octahedral CoO_6 with low crystal fields contribute to creation of a window for blue transmission. Then a new generation of blue pigment with a low cobalt rate, on the basis of the Co-doped $ZnMoO_4$ composition, can be prepared.

AUTHOR INFORMATION

Corresponding Author

*E-mail: demourg@icmcb-bordeaux.cnrs.fr.

REFERENCES

(1) Llusar, M.; Forès, A.; Badenes, J. A.; Calbo, J.; Tena, M. A.; Monros, G. *J. Eur. Ceram. Soc.* **2001**, *21*, 1121.
(2) Perrez-Bernal, M. E.; Ruano-Casero, R. J.; Rives, V. *J. Solid State Chem.* **2009**, *182*, 2566–2578.
(3) Kuzian, R. O.; Daré, A. M.; Sati, P.; Hayn, R. *Phys. Rev. B* **2006**, *74*, 155201.
(4) Rojo, J. M.; Mesa, J. L.; Pizarro, J. L.; Lezama, L.; Arriortua, M. I.; Rojo, T. *J. Solid State Chem.* **1997**, *132*, 107–112.
(5) Messeguer, S.; Tena, M. A.; Gargori, C.; Badenes, J. A.; Llusar, M.; Monros, G. *Ceram. Int.* **2007**, *33*, 843–849.
(6) Gaudon, M.; Apheiceixborde, A.; Ménétrier, M.; Demourgues, A. *Inorg. Chem.* **2009**, *48*, 9085–9091.
(7) Gaudon, M.; Toulemonde, O.; Demourgues, A. *Inorg. Chem.* **2007**, *46*, 10996–11002.
(8) Klaska, K. H.; Eck, J. C.; Pohl, D. *Acta Crystallogr., B* **1978**, *34*, 3324–3325.
(9) Brunold, J .C.; Gudel, H. U.; Cavalli, E. *Chem. Phys. Lett.* **1996**, *252* (1−2), 122–120.
(10) Pozas, R.; Orera, V. M.; Ocana, M. *J. Eur. Ceram. Soc.* **2005**, *25* (13), 3165–3172.
(11) Nord, A. G.; Stefanidis, T. *Acta Chem. Scand., A* **1983**, *37*, 715–721.
(12) Harrison, W. T. A.; Vaughey, J. T.; Dussack, L. L.; Jacobson, A. J.; Martin, T. E.; Stucky, G. D. *J. Solid State Chem.* **1995**, *114*, 151.
(13) Rojo, J. M.; Mesa, J. L.; Lezama, L.; Barberis, G. E.; Rojo, T. *J. Magn. Magn. Mater.* **1996**, *157/158*, 493–495.
(14) Miyake, M.; Nakamura, H.; Kojima, H.; Marumo, F. *Am. Mineral.* **1987**, *72*, 594–598.
(15) Sleight, A. W.; Chamberland, B. L. *Inorg. Chem.* **1968**, *7* (8), 1672–1675.
(16) Rodriguez, J. A.; Chatuvedi, S.; Hanson, J. C.; Albornoz, A.; Brito, J. L. *J. Phys. Chem. B* **1998**, *102*, 1347–1355.
(17) Gaudon, M.; Demourgues, A.; Deniard, P.; Thiry, A. E.; Carbonera, C.; Le Nestour, A.; Largeteau, A.; Létard, J. F.; Jobic, S. *Adv. Mater.* **2007**, *19*, 3517–3519.
(18) Gaudon, M.; Carbonera, C.; Thiry, A. E.; Demourgues, A.; Deniard, P.; Payen, C.; Letard, J. F.; Jobic, S. *Inorg. Chem.* **2007**, *46* (24), 10200–10207.
(19) Gaudon, M.; Thiry, A. E.; Largeteau, A.; Deniard, P.; Jobic, S.; Majimel, J.; Demourgues, A. *Inorg. Chem.* **2008**, *47* (7), 2404–2410.
(20) Abrahams, S. C. *J. Chem. Phys.* **1967**, *46* (6), 2052–2063.

(21) Reichelt, W.; Weber, T.; Sohnel, T.; Dabritz, S. *Z. Anorg. Allg. Chem.* **2000**, *626*, 2020–2027.
(22) Rietveld, H. M. *J. Appl. Crystallogr.* **1969**, *2*, 65.
(23) Brown, I. D.; Altermatt, D. *Acta Crystallogr., B* **1985**, *41*, 244–247.
(24) Abragam, A.; Pryce, M. H. L. *Proc. R. Soc. London, A* **1951**, *206*, 173.
(25) Harris, E. A. *Phys. Chem. Glasses* **1987**, *28*, 196.
(26) Villeneuve, G.; Pizarro, J. L.; Dance, J. M.; Arriortua, M. I.; Rojo, T.; Kuentzler, R. *J. Magn. Magn. Mater.* **1990**, *83*, 478–480.
(27) Borrás-Almenar, J. J.; Coronado, E.; Gatteschi, D.; Zanchini, C. *Inorg. Chem.* **1992**, *31*, 294–298.